Karlsruhe Institute of Technology

Elektrotechnisches Institut (ETI)
Prof. Dr.-Ing. Michael Braun
Prof. Dr.-Ing. Martin Doppelbauer
Prof. Dr.-Ing. Marc Hiller
Kaiserstr.12. 76131 Karlsruhe

Elektrotechnisches Institut

Title:	Determining the volume optimal parameter values for multi-phase permanent magnet synchronous motors with switchable coil configuration
Authors:	Miriam Boxriker, Johannes Kolb, Martin Doppelbauer
Institute:	Karlsruhe Institute of Technology (KIT) Elektrotechnisches Institut (ETI) Hybrid Electric Vehicles (HEV)
Type:	Conference Proceedings
Published at:	2018 20th European Conference on Power Electronics and Applications (EPE'18 ECCE Europe), Riga, Latvia Publisher: IEEE, Piscataway (NJ) Year: 2018 ISBN: 978-90-75815-28-3 Pages: 1-9
Hyperlinks:	Scopus: https://www.scopus.com/record/display.uri?eid=2-s2.0-85057034485&origin=resultslist

Determining the Volume Optimal Parameter Values for Multi-Phase Permanent Magnet Synchronous Motors with Switchable Coil Configuration

Miriam Boxriker, Johannes Kolb*, Martin Doppelbauer
Karlsruhe Institute of Technology (KIT) - Elektrotechnisches Institut (ETI)
Kaiserstr. 12, 76131 Karlsruhe, Germany
Phone: +49 (0) 721 608-42700
Email: miriam.boxriker@kit.edu
URL: www.eti.kit.edu
* Schaeffler Technologies AG & Co. KG - SHARE at KIT

Keywords

≪Permanent magnet motor≫,≪Multiphase drive≫,≪Synchronous motor≫,≪Electrical machine≫, ≪Electric Vehicle≫

Abstract

This contribution suggests an approach to determine the optimal parameter values of permanent magnet flux linkage and saliency ratio of Permanent Magnet Synchronous Motors with multi-phase windings and coil configuration switching. Therein, their influence on volume is calculated analytically for both motor and power electronics in a unified manner identifying promising designs. Of the exemplary design parameters, a maximum volume reduction of 27% can be achieved. An experimental validation supports the analytic calculation of the motor torque vs. speed behavior.

Introduction

A driving topic in the development of the electric propulsion system in modern electric and hybrid electric vehicles is the improvement of power density because a reduction of volume and weight promises an increase in the cruising range [1,2]. Permanent Magnet Synchronous Motors (PMSM) are well suited to fulfill this task [3]. Nevertheless, there are efforts to improve the performance of the motor further. One approach is the rise in applicable coil configurations, as e.g. with a star-delta-configuration switching [4]. The possible expansion in operating range is shown in [5]. Multi-phase windings are also proposed to deal with it [6–8]. They improve the usage of the DC-link voltage at space vector pulse width modulation, reduce the common mode voltage while enhancing the electromagnetic coupling of stator and rotor [6].

[9] introduced a way to calculate the effects of both options analytically in relation to each other with a rough estimation of the additional effort isolated on the semiconductors. Since the volume of the whole propulsion system is the crucial value to optimize, this contribution focuses on the analytical determination of the entire change in volume by coil configuration switching and multi-phase windings of both the motor and the power electronics. The analytical approach holds the advantage, that no time consuming optimization process with Finite Element Analysis has to be carried out with a huge number of input values to identify the area of interest or to exclude some designs or options. The approach is done by the extended parameter plane [5,9,10], which calculates the torque speed characteristic dependent on the permanent magnet flux linkage and the saliency of a motor in the right relation to each other. With the results and a base motor and power electronics design, the difference in the needed apparent power and the output power results in changed volume demands. These deviations and promising areas are presented in this paper.

In this contribution, the parameter plane and its extension are first described shortly. In the following section, the equations and the procedure for determining the volume change of the motor and the converter due to the coil configuration switching and multi-phase windings are submitted. Afterwards, the procedure is applied using an assessment criterion and a base design for the evaluation is chosen. The analytical results are introduced thereafter. This contribution concludes with an experimental setup and testbench results for validating the extended parameter plane.

Extended Parameter Plane

[10] proposed the parameter plane as basis for the calculation of the torque speed characteristic of motors. It can be calculated by only two parameters, the permanent magnet flux linkage ψ_{PM} and the saliency ζ, which is the ratio of the quadrature inductance L_{q} to the direct inductance L_{d} under some assumptions as linear material characteristics, a neglect of losses and sinusoidal excitation [10].

In a second step, the motor values are normalized with the result that the maximum current $i_{\max}$, the maximum voltage $v_{\max}$, the maximum ideal torque t and power p are set to one [10] allowing the determination of the torque speed characteristic for each tuple of ψ_{PM} and ζ with eq. (3), eq. (4) and eq. (5). The field weakening area therefore starts at speed $\omega = 1$. An exemplary result is given in Fig. 1 a).

If e.g. the results of the coil configuration switching are to be assessed, the original parameter plane cannot be used but has to be extendend [5, 9]. In this contribution, the variables taken into account are the phase number m, the number of windings in series per phase w and the winding factor ξ. Since the dependence of the normalized inductances $l_{\mathrm{d,q}}$ and ψ_{PM} can be written as [9]

$$l_{\mathrm{d,q}} \propto m \cdot w^2 \cdot \xi^2 \qquad (1) \qquad \text{and} \quad \psi_{\mathrm{PM}} \propto w \cdot \xi, \qquad (2)$$

ratio factors describing the change to a base design are introduced. This is done in that way, that it results in $k_{\mathrm{w}} = \frac{w}{w_{\mathrm{b}}}$ for coil configuration changes, $k_{\xi} = \frac{\xi}{\xi_{\mathrm{b}}}$ for winding factor changes and $k_{\mathrm{m}} = \frac{m}{m_{\mathrm{b}}}$ for phase number changes [9]. Therein, the index b marks the base design value for the phase number, the winding factor or the number of windings in series per phase. The ratio factors themselves can attain values between $0 < k_{x|x=w,\xi,m} \leq 1$ and the original motor equations [10] on the left hand side are extended to those on the right hand side [9]:

$$v_{\mathrm{d}} = -\omega\zeta l_{\mathrm{d}} i_{\mathrm{q}} \quad (3) \quad \rightarrow \quad v_{\mathrm{d}} = -k_{\mathrm{w}}^2 k_{\xi}^2 k_{\mathrm{m}}\, \omega\zeta l_{\mathrm{d}} i_{\mathrm{q}} \quad (6)$$

$$v_{\mathrm{q}} = \omega l_{\mathrm{d}} i_{\mathrm{d}} + \omega\psi_{\mathrm{PM}} \quad (4) \quad \rightarrow \quad v_{\mathrm{q}} = k_{\mathrm{w}}^2 k_{\xi}^2 k_{\mathrm{m}}\, \omega l_{\mathrm{d}} i_{\mathrm{d}} + k_{\mathrm{w}} k_{\xi}\, \omega\psi_{\mathrm{PM}} \quad (7)$$

$$t = \psi_{\mathrm{PM}} i_{\mathrm{q}} - (\zeta - 1) l_{\mathrm{d}} i_{\mathrm{d}} i_{\mathrm{q}} \quad (5) \quad \rightarrow \quad t = k_{\mathrm{w}} k_{\xi} / k_{\mathrm{m}}\, \psi_{\mathrm{PM}} i_{\mathrm{q}} - k_{\mathrm{w}}^2 k_{\xi}^2\, (\zeta - 1) l_{\mathrm{d}} i_{\mathrm{d}} i_{\mathrm{q}} \quad (8)$$

where v_{d} and v_{q} are the normalized voltages in d- and q-axis and i_{d} and i_{q} are the normalized currents respectively. If the number of phases is changed from three to m, it is assumed in this contribution that the number of windings per coil has to be increased by $m/3$ to get the same winding number w at a reduced phase current $i_{\max} = i_{\max,\mathrm{b}}/k_{\mathrm{m}}$ [9]. The result of torque speed characteristics calculated with the extended equations is shown in Fig. 1 c).

The design space of the extended parameter plane is however restricted by the maximum allowed induced voltage as depicted in Fig. 1 b). If the induced voltage increases above the maximum blocking voltage of the semiconductors v_{br}, this would lead to their destruction. The equation for the maximum induced voltage v_{ind} at maximum speed ω_{end} for normal multi-phase systems can be written as [9]

$$v_{\mathrm{ind}} = k_{\mathrm{w}} k_{\xi}\, \omega_{\mathrm{end}}\, \psi_{\mathrm{PM}} \sqrt{2\left(1 - \cos\left(\frac{m-1}{m}\pi\right)\right)} \qquad (9)$$

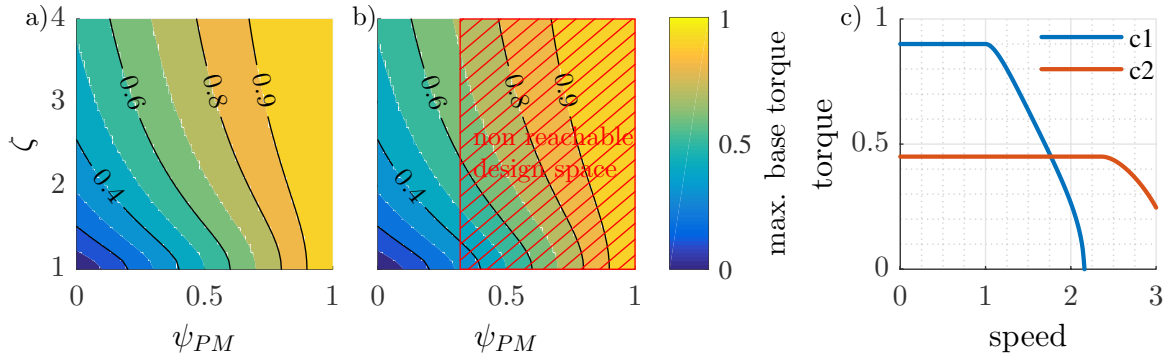

Fig. 1: a) Result of the parameter plane regarding the maximum base torque. b) The maximum induced voltage constraining the design space. c) Torque speed characteristics c1 and c2 obtained by the extended parameter plane at $\psi_{\mathrm{PM}} = 0.9$ and $\zeta = 1$ with c1: $k_{\mathrm{w}} = 1$, $k_{\mathrm{m}} = 1$, $k_{\xi} = 1$ and c2: $k_{\mathrm{w}} = 0.5$, $k_{\mathrm{m}} = 1/3$, $k_{\xi} = 0.96$

Calculation of the Motor and Converter Volumes

The previous section established the baseline for the estimation of the volume. For the calculation itself, some further assumptions have to be made: The material characteristics and cooling mechanism and therefore the cooling ability are not changed during the comparison. Moreover having the same coil pitches, the dimensions of the motor (stator outer diameter, end winding, housing,...) therefore scale to the inner stator volume. Regarding radial flux motors, the inner volume of the stator is proportional to the torque [14]. This is set in relation to a criterion value C - it will be explained in more detail in the next section - which describes the performance of the motor. For the comparison, a base design ($\psi_{\mathrm{PM,base}}$ and ζ_{base}) with C_{base} is chosen which sets the requirements for other designs. If the criterion value C_{base} is exceeded by other designs, they can reach the same value with lower apparent power, that means that $p = u \cdot i$ is lowered by the same ratio ρ as C_{base} is exceeded (see eq. (10)). As the ideal motor is proportional to a volume, this means also a reduction in motor volume Vol_{mot} compared to the base design volume $Vol_{\mathrm{mot,base}}$.

$$p = \frac{C_{\mathrm{base}}}{C} \cdot p_{\mathrm{base}} = \rho \cdot p_{\mathrm{base}} \qquad (10) \qquad Vol_{\mathrm{mot}} = \frac{C_{\mathrm{base}}}{C} \cdot Vol_{\mathrm{mot,base}} = \rho \cdot Vol_{\mathrm{mot,base}} \qquad (11)$$

The volume of the converter is significantly determined by the cooling [13]. Hence, the maximum losses of the converter are taken as a measure of the volume of the converter itself. These losses consist in good approximation of conduction and switching losses [15]. As shown in [6], the power losses in m-leg-inverters with IGBTs and diodes stay the same for different m if the same semiconductor area is used. This can also be applied to MOSFETs, which are used as semiconductor switches in this contribution. With the equations from [15], the conduction losses for one MOSFET $P_{\mathrm{cond,MOSFET}}$ are

$$P_{\mathrm{cond,MOSFET}} = \left(\frac{2}{8} + \frac{\alpha \cdot \cos(\phi)}{3\pi} - \frac{\alpha \cdot \cos(\phi)}{3\pi} \right) \cdot R_{\mathrm{DSon}} \cdot \hat{i}^2 = \frac{1}{4} \cdot R_{\mathrm{DSon}} \cdot \hat{i}^2 \qquad (12)$$

if the MOSFET is conducting both current directions. R_{DSon} is the channel resistance of the MOSFET, α is the modulation degree and $\cos(\phi)$ is the power factor. This leads to the conduction losses of an m-leg inverter P_{cond} to eq. (13). Hereby, the R_{DSon} for $m = 9$, $R_{\mathrm{DSon,m9}}$, has to be 3 times higher than the R_{DSon} for $m = 3$, $R_{\mathrm{DSon,m3}}$, due to the assumed same semiconductor area. $R_{\mathrm{DSon,m3}}$ is set to R_{DSon} in the following for a better readability. The current i is simultaneously reduced by that factor. To simplify the equations, the switching losses of the base design $P_{\mathrm{sw,base}}$ are only given with the ratio x_1 of $P_{\mathrm{cond,base}}$ (eq. (14)):

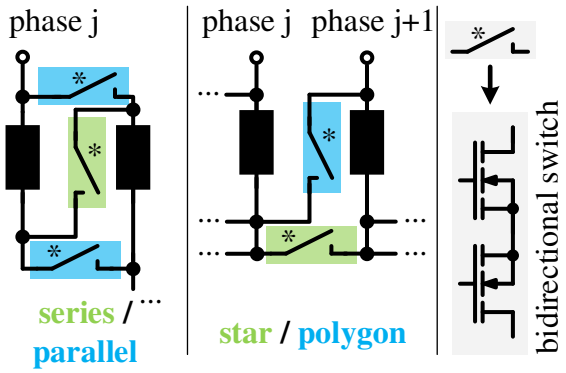

Fig. 2: Exemplary switching options with bidirectional switches

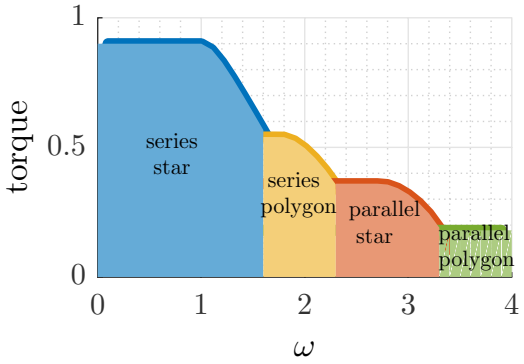

Fig. 3: Switched on areas of exemplary configurations shown with different colors

$$P_{\text{cond}} = \frac{m}{2} \cdot \left(\frac{m}{3} \cdot R_{\text{DSon,m3}}\right) \cdot \left(\frac{3}{m} \cdot \hat{i}\right)^2 = \frac{3}{2} \cdot R_{\text{DSon}} \cdot \hat{i}^2 \quad (13) \qquad P_{\text{sw,base}} = x_1 \cdot P_{\text{cond,base}} \quad (14)$$

These equations contain the option to find an optimum under a reduced parameter set, which is nevertheless adaptable to the behavior of distinct semiconductors if necessary. Due to the linear dependency of P_{sw} on i and the quadratic dependency of P_{cond} on i [15], the volume of the power electronics needed by a certain design $P_{\text{loss,pe}}$ can be written with $P_{\text{loss,pe,base}} = 1$

$$P_{\text{loss,pe,base}} = P_{\text{sw,base}} + P_{\text{cond,base}} = (x_1 + 1) P_{\text{cond,base}} \stackrel{!}{=} 1 \quad \rightarrow \quad P_{\text{cond,base}} = \frac{1}{1 + x_1} \quad (15)$$

$$P_{\text{loss,pe}} = \rho \cdot P_{\text{sw,base}} + \rho^2 \cdot P_{\text{cond,base}} = \rho \frac{x_1}{1 + x_1} + \rho^2 \frac{x_1}{1 + x_1} = \rho \frac{x_1 + \rho}{1 + x_1} \quad (16)$$

If fixed coil configurations are used, eq. (16) provides the estimation of the converter volume. If coil configurations are switched (see Fig. 2 cf. [9]), additional conduction losses occur caused by the bidirectional switches. Switching losses can be neglected for those semiconductors as their switching frequency is substantially lower than the switching frequency of the m-leg-inverter. Since only one configuration is switched on and is consequently the only one producing losses at one point of time (with the neglect of blocking losses), the configuration with the highest losses dimensions the needed volume. Exemplary areas for the conduction losses of one configuration are given in Fig. 3, where one color depicts the switched on state of one coil configuration. The number of bidirectional switches of this configuration is given by $n_{\text{bs,state}}$. By implication, this also means that the used MOSFETs for the bidirectional switches can be only chosen due to their low $R_{\text{DSon,csw}}$ without considering switching losses. $R_{\text{DSon,csw}}$ can therefore be given by a ratio x_2 compared to the R_{DSon} of the m-leg-inverter. This leads to the equation of the power electronics volume $\text{Vol}_{\text{pe,csw}}$, which includes the converter and the coil configuration switching unit:

$$\text{Vol}_{\text{pe,csw}} = \rho \cdot \frac{\rho\,(3 + x_2 x_{\text{sw}})\,3x_1}{3 + 3x_1} \qquad \text{with} \qquad R_{\text{DSon,csw}} = x_2 \cdot R_{\text{DSon}} \quad (17)$$

x_{sw} hereby contains the ratio of the conduction losses of the coil configuration switching unit to the conduction losses of the base m-leg-inverter (see eq. (18)). The values are shown in Table I. The laws of volume growth by calculation of the maximum conduction power losses are introduced by [12] and one possible application appears in [9]. For this contribution, the current is set as scaling value which leads to slightly different values than in [9]:

Table I: Design Choices (Serial(Ser),Parallel(Par),Star(Y),Δ and Polygon(PG) configuration), x_{sw} and $x_{\mathrm{sw,ext}}$

Design no.	m	Switching	$\max\{P_{\mathrm{cond}}\}$state	$n_{\mathrm{bs,state}}$	$\mathrm{Vol}_{\mathrm{config.}}$	x_{sw}	$x_{\mathrm{sw,ext}}$
1	3	Y / Δ	Y	$m-1$	1.88 $\mathrm{Vol}_{\mathrm{3PB,base}}$	4	3.79
2	3	Ser / Par / Y / Δ	Ser+Y	$2m-1$	2.94 $\mathrm{Vol}_{\mathrm{3PB,base}}$	10	9.29
3	9	Ser / Par / Y / 3xPG	Ser+Y	$2m-1$	6.11 $\mathrm{Vol}_{\mathrm{3PB,base}}$	3.778	4.01

$$x_{\mathrm{sw}} = \max\left\{\frac{P_{\mathrm{cond,csw}}}{P_{\mathrm{cond}}}\right\} = 2\cdot n_{\mathrm{bs,state}}\cdot\left(\frac{i_{\max}}{i_{\max,\mathrm{b}}}\right)^2 = 2\cdot n_{\mathrm{bs,state}}\cdot\left(\frac{3}{m}\right)^2 \tag{18}$$

Since the calculation of the maximum conduction power losses of the coil configurations does not take into account a growth in switching options with lower power losses than in the configuration with the maximum losses, an additional criterion punishes the growth in the overall semiconductor volume. eq. (20) provides the fundamental calculation rule for the cost function embodied by $x_{\mathrm{sw,ext}}$ which is an extension to the previous introduced x_{sw} (cf. eq. (18)). The cost factors are chosen because of the different influence of cooling and passives and semiconductors on the volume. According to [13], a typical converter volume consists of about 90% of cooling and passives and 10% of semiconductor if only components themselves and not air are considered.

Knowing the relation in volume between the base motor x_{mot} and the base power electronics x_{pe} (e.g. due to a commercial propulsion system), the overall volume of motor and converter $\mathrm{Vol}_{\mathrm{sum}}$ can be written as

$$\mathrm{Vol}_{\mathrm{sum}} = \rho\cdot\left(x_{\mathrm{mot}} + x_{\mathrm{pe}}\frac{\rho\,(3+x_2x_{\mathrm{sw,ext}})\,3x_1}{3+3x_1}\right) \quad \text{with} \quad \mathrm{Vol}_{\mathrm{sum,base}} = x_{\mathrm{mot}} + x_{\mathrm{pe}} = 1 \tag{19}$$

$$\text{with} \quad x_{\mathrm{sw,ext}} = 0.9\cdot x_{\mathrm{sw}} + 0.1\cdot\frac{\mathrm{Vol}_{\mathrm{config.}}}{\mathrm{Vol}_{\mathrm{3PB,base}}} \tag{20}$$

with the semiconductor volume of the base design 3-leg-inverter $\mathrm{Vol}_{\mathrm{3PB,base}}$ and the semiconductor volume of the inverter and the coil configuration $\mathrm{Vol}_{\mathrm{config}}$.

Application of Procedure

For applying the introduced procedure, a base design of a motor with a corresponding power electronics has to be chosen, which delivers the base volume and maximum values of current and voltage. Moreover, the criterion value C has to be defined determining the performance of a motor design in one parameter. One option for the respective calculation is introduced in the following: the operating-range-criterion.

Operating Range Criterion

The operating-range-criterion A_{Pn} can be chosen as the criterion value C giving the ratio of the area under the torque speed characteristic compared to the area of the ideal torque speed characteristic [5]:

$$A_{\mathrm{Pn}} = \frac{\int_0^{\omega_{\mathrm{end}}} t_{\max}(\omega, k_{x|x=w,\xi,m})\mathrm{d}\omega}{\int_0^{\omega_{\mathrm{end}}} t_{\mathrm{ideal}}(\omega)\mathrm{d}\omega} \quad \text{and} \quad 0 \le A_{\mathrm{Pn}} \le 1 \tag{21}$$

whereby $t_{\max}$ is the maximum torque concerning k_{x} for one design at a specific speed ω and t_{ideal} is the torque of an ideal motor. Fig. 4 depicts the operating range criterion A_{Pn}.

Base Design

The base motor and power electronics designs are created by parameters of an available commercial design for EVs [16]. The maximum torque speed characteristics are approximated to get the $\psi_{\mathrm{PM,base}}$ and ζ_{base}. With this a mean value of $\psi_{\mathrm{PM,base}} = 0.41$ and $\zeta_{\mathrm{base}} = 2.4$ can be stated.

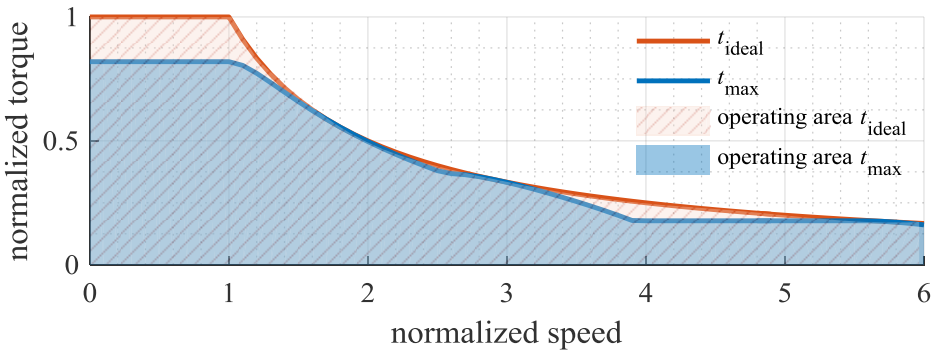

Fig. 4: The area of the torque(t_{max})-speed-curve of an exemplary configuration and the area of the ideal characteristic illustrating the calculation of A_{Pn} [9]

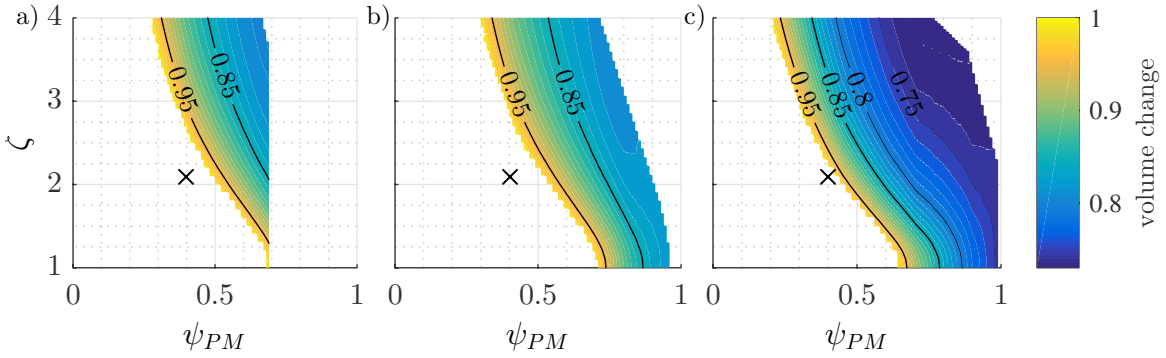

Fig. 5: a) Volume decrease of design 1 compared to the base design, b) volume decrease of design 2 compared to the base design, c) volume decrease of design 3 compared to the base design.

As the total volume of power electronics and motor is set to 1 for the base design, this leaves 0.688 and 0.312 for x_{mot} and x_{pe} respectively with the data of [16]. The maximum induced voltage is used as a constraint for the parameter plane. Moreover, the ratio of the maximum speed ω_{end} to the maximum base speed ω_0 is about 3 for the designs. Often, the semiconductors are designed in that way that the conduction losses in the power electronics equal the switching losses. Therefore, x_1 is also set to 1. However, the case is different for the switching unit. As the frequency of the configuration switching is very small compared to the one in the power electronics, semiconductors only optimized for low conduction losses can be chosen. This reduces the R_{DSon} in this example by $x_2 = 0.1$. $k_{u,safe}$ gives the safety margin between $v_{ind,max}$ and v_{br}: $v_{br} = k_{u,safe} \cdot v_{ind,max}$, which is set here to 1.2 [16]. The total volume for different designs in the parameter plane can now be calculated with eq. (19) and the parameter defined in Table II.

Table II: Choice of Parameters

Parameter	x_{mot}	x_{pe}	x_1	x_2	C_{base}	$k_{u,safe}$	ω_{end}/ω_0
Value	0.688	0.312	1	0.1	0.7309	1.2	3

Results of the Analytic Approach

The results for the design choices are shown in Fig. 5 a), b) and c).

Hereby, only the designs fulfilling the maximum induced voltage constraint and with a volume reduction are depicted. Moreover, the figures represent a Pareto optimality: Designs which are dominated by others in volume reduction, in smaller ζ or ψ_{PM} are also not considered. The 'x' indicates the base design parameters. Comparing the two three-phase designs, it can be stated, that the star-delta-switching

(Fig. 5 a)) already pays off at lower ψ_{PM} than that design with the additional series-parallel switching (Fig. 5 b)). Besides, the maximum achievable gain in volume is also higher (19.3 % compared to 18.5 %). In spite of that, the design 2 performs better than design 1 at ψ_{PM} higher than 0.75 and ζ smaller than 2. If the $m = 9$ design in Fig. 5 c) is compared to the $m = 3$ designs, it can be seen, that it is superior to both in the achievable area as well as in the maximum volume reduction of 27%. All in all, it can be asserted that improvements in volume are possible due to a higher saliency. The effect however is reduced at rising ψ_{PM} (cf. Fig. 5 b) and c)). Nevertheless, a high saliency cannot compensate for a very low ψ_{PM}. Moreover, the more switching options the higher ψ_{PM} values can be reached leading to a volume reduction at small ζ. Furthermore, less switching options can lead to an improved volume reduction compared to more switching configurations (cf. $m = 3$ designs). Therefore, the number of switching options has to be chosen carefully for a distinct application.

Experimental Validation of the Extended Parameter Plane

A prototype, called device under test (DUT) in the following, and a converter were built up to validate the calculation of the extended parameter plane. The DUT is a PMSM with surface magnets and concentrated windings. It is built with an open coil configuration so that the coils can be connected in different ways. The motor can realize three and nine phase configurations due to its number of slots and pole pair number. The machine data is summed up in Table III. Fig. 6 a) shows the nine-leg-inverter feeding the DUT and Fig. 6 b) the prototype motor. The testbench converter signal processing devices are explained in [11]. The measurements are realized with a Yokogawa WT3000, whereby the currents are measured with high precision current sensors. For the three phase motor, this is sufficient for all input values. For the nine phase configuration, only one 3 phase system out of 3 is measured. This is valid due to the current and voltage symmetry. The torque and speed of the motor are measured by a torque measuring flange which transmits the measured data to the Yokogawa WT3000.

Table III: Machine Data

Data	Value
rated current	10.5A
DC-link voltage $m = 3$	74.3V
DC-link voltage $m = 9$	23.8V
coil winding number	32
number of slots	36
winding factor $m = 3$	0.9525
winding factor $m = 9$	0.9923
pole pair number	17

Winding configuration $m = 3$, $m = 9$

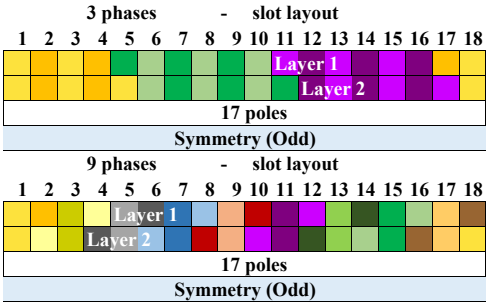

a) b)

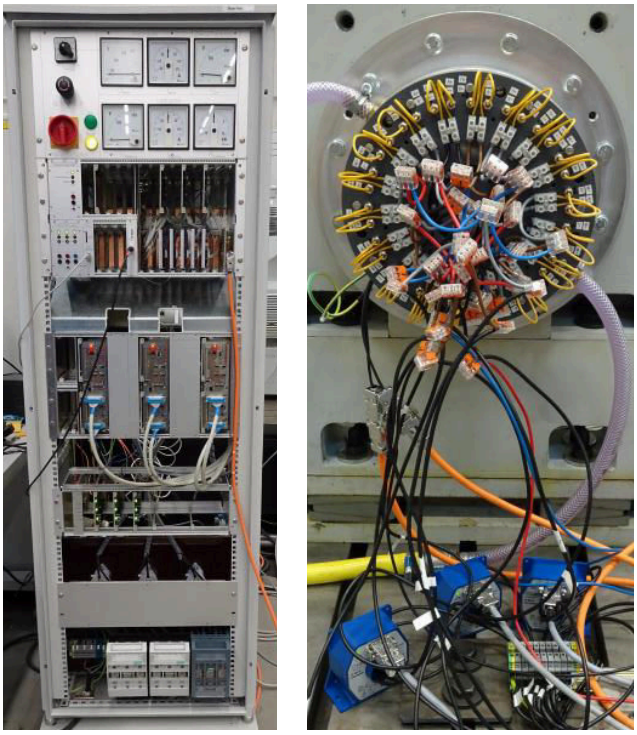

Fig. 6: a) Nine-leg inverter and b) Prototype

Prototype Configurations

Concerning the prototype, there are 36 coils, which means that there are twelve coils per phase for a three phase configuration and four coils per phase for a nine phase configuration. As circulating currents

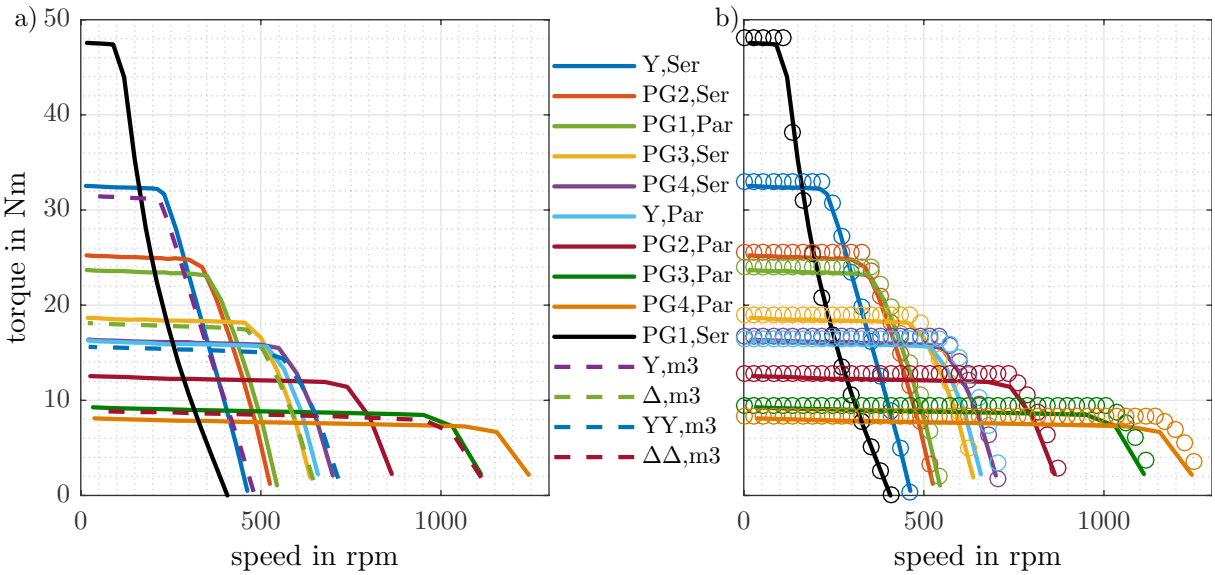

Fig. 7: Results of measurements: a) all configurations of 3 and 9 phases, b) comparison of 9 phase configuration measurements (solid lines) and their analytic calculation (circles). The stator resistance is included in the analytic calculation for the comparison.

due to different induced voltages shall be prevented, coils can be only connected in parallel if the angle to a rotor pole at a certain step of time is the same. This means for the motor, that there is one parallel configuration for $m = 3$ as well as for $m = 9$ (cf. Table III Winding configurations). As introduced in [5], this leads to a total number of configurations for the 3-phase motor of 4 configurations: a Wye- and a Delta-connection carried out in series or with two parallel groups of six coils in series. The 9-phase motor consists of 10 configurations in total: one Wye- and four polygon connections, where the coils of a phase are all in series or where two groups consisting of two coils in series are connected in parallel. For the measurements of the prototype, the DC-link-voltage is reduced for the 9-phase configuration to get the same input power as for the three phase configuration. The current cannot be reduced because the coil winding number cannot be changed. If that was possible, the current could be reduced by simultaneously increasing the coil winding number by the same amount.

Validation results

Fig. 7 depicts the measurement results of the prototype. The maximum measured torque speed characteristics with the given input parameters (cf. Table III) are shown in Fig. 7 a). The 9-phase characteristics are represented by solid lines and the 3-phase ones in dashed lines. Since the 9-phase motor can utilize the DC-link-voltage better than a 3-phase motor with a Space Vector Pulse Width Modulation [6], the DC-link-voltage for $m = 9$ is not only reduced by 3 compared to $m = 3$ but by 3.12 in order to lead to the same maximum base speed ω_0. As can be seen, the maximum torque of the nine phase configuration is higher than the corresponding three phase configuration. Due to the reduction of the DC-link-voltage, there is a intersection of the respective $m = 3$ and $m = 9$ curves. This can be avoided by using a DC-link-voltage for $m = 9$ which is a exactly a third of the DC-link-voltage for $m = 3$.

Fig. 7 b) depicts the measured torque speed characteristics of the nine phase motor in solid lines compared to the analytic calculation of the extended parameter plane in circles. The colors of the lines and circles correspond to the legend of Fig. 7 a). The calculation obviously matches the measurement very well. The voltage drop at the stator resistance is considered in the analytic calculation for this comparison because it cannot be neglected for the prototype. The voltage drop is within in the range of a fourth of the stator voltage at maximum base speed (Wye-configuration). Calculation and measurement deviate from each other for increasing speed. The reason for this behavior is based on the neglect of friction and iron losses in the extended parameter plane.

Conclusion

This contribution presents a way of analytically assessing the changes in volume evoked by multi-phase windings and coil configuration switching. This is used to predict areas where the higher effort of these two options leads to an improvement of the propulsion unit culminating in a maximum volume reduction of 27%. The calculations of the extended parameter plane are validated by measurements. The torque speed characteristics show a very good accordance to the analytical calculation. The occurring difference can be explained by friction and iron losses which are not implemented in the analytical calculation.

References

[1] S. Rogers, U.S. Departement of Energy: (2017, April 25), *Advanced Power Electronics and Electric Motors R&D* [Online]. Available: https://energy.gov/sites/prod/files/2014/03/f13/ape00a_rogers_2013_o.pdf

[2] S. Günther, S. Ulbrich, W. Hofmann, *Driving cycle-based design optimization of interior permanent magnet synchronous motor drives for electric vehicle application*, 2014 International Symposium on Power Electronics, Electrical Drives, Automation and Motion (SPEEDAM), 2014

[3] T. Finken, M. Hombitzer, K. Hameyer, *Study and comparison of several permanent-magnet excited rotor types regarding their applicability in electric vehicles*, Emobility - Electrical Power Train, 2010

[4] E. Nipp, *Permanent Magnet Motor Drives with Switched Stator Windings*, PhD Thesis, Stockholm, 1999.

[5] M. Boxriker, P. Winzer, J. Kolb and M. Doppelbauer, *Increasing the Operating Range of Permanent Magnet Synchronous Motors by Switching the Winding Configurations*, IEEE 2nd Annual Southern Power Electronics Conference, 2016, pp.1-6

[6] M. Boxriker, J. Kolb and M. Doppelbauer, *Expanding the Operating Range of Permanent Magnet Synchronous Motors by Using the Optimum Number of Phases*, 18th European Conference on Power Electronics and Applications, 2016, pp.1-8

[7] L. Parsa, *On Advantages of Multi-Phase Machines*, 31st Annual Conference of IEEE Industrial Electronics Society, IECON, 2005, 6 pp.

[8] Y. Burkhardt, A. Spagnolo, P. Lucas, M. Zavesky and P. Brockerhoff, *Design and analysis of a highly integrated 9-phase drivetrain for EV applications*, IEEE Transactions on Industrial Electronics, 2008, pp. 1893 - 1909

[9] M. Boxriker, J. Kolb and M. Doppelbauer, *Effects of Coil Configuration Switching, Pole-Changing and Multi-Phase Windings on Permanent Magnet Synchronous Motors*, 43rd Annual Conference of the IEEE Industrial Electronics Society (IECON), 2017, pp.1925-1932

[10] W. L. Soong, *Design and Modelling of Axially-Laminated Interior Permanent Magnet Motor Drives for Field-Weakening Applications*, PhD Thesis, Glasgow, 1993.

[11] C. Axtmann, M. Boxriker and M. Braun, *A Custom, High-Performance Real Time Measurement and Control System for Arbitrary Power Electronic Systems in Academic Research and Education*, 18th European Conference on Power Electronics and Applications, 2016, pp.1-7

[12] T. Bülo, *Methode zur Evaluation leistungselektronischer Schaltungstopologien für die Anwendung in dezentralen Netzeinspeisern kleiner Leistung*, Dissertation, Kassel University Press, Kassel, 2010

[13] M. März, A. Schletz, B. Eckardt, S. Egelkraut, H. Rauh, *Power Electronics System Integration for Electric and Hybrid Vehicles*, 6th International Conference 2010 on Integrated Power Electronics Systems, 2010

[14] G. Müller, K. Vogt and B. Ponick, *Berechnung elektrischer Maschinen*, 6th edition, WILEY-VCH Verlag GmbH & Co. KGaA, Weinheim, 2008.

[15] A. Wintrich, U. Nicolai, W. Tursky, T. Reimann, SEMIKRON International GmbH: (2017, December 1), *Application Manual Power Semiconductors* [Online]. Available: https://www.semikron.com/dl/service-support/downloads/download/semikron-application-manual-power-semiconductors-english-en-2015/

[16] BRUSA Elektronik AG: (2017, December 1), *Power Electronics DMC524 and PSM HSM1-6.17.12* [Online]. Available: http://www.brusa.biz/en/products/drive/controller-400-v/dmc524.html and http://www.brusa.biz/en/products/drive/motor-400-v/hsm1-61712.html